NANO LETTERS

LETTER

pubs.acs.org/NanoLett

Atomic-Resolution Imaging of Spin-State Superlattices in Nanopockets within Cobaltite Thin Films

Jaume Gazquez,[*,†,‡] Weidong Luo,[§,‡] Mark P. Oxley,[§,‡] Micah Prange,[§,‡] Maria A. Torija,[∥] Manish Sharma,[∥] Chris Leighton,[∥] Sokrates T. Pantelides,[§,‡] Stephen J. Pennycook,[‡] and Maria Varela[‡]

[†]Departamento de Física Aplicada III, Universidad Complutense de Madrid, Madrid, 28040, Spain

[‡]Materials Science and Technology Division, Oak Ridge National Laboratory, Oak Ridge, Tennessee 37831, United States

[§]Department of Physics and Astronomy, Vanderbilt University, Nashville, Tennessee 37235, United States

[∥]Department of Chemical Engineering and Materials Science, University of Minnesota, Minneapolis, Minnesota 55455, United States

ABSTRACT: Certain cobalt oxides are known to exhibit ordered Co spin states, as determined from macroscopic techniques. Here we report real-space atomic-resolution imaging of Co spin-state ordering in nanopockets of $La_{0.5}Sr_{0.5}CoO_{3-\delta}$ thin films. Unlike the bulk material, where no Co spin-state ordering is found, thin films present a strain-induced domain structure due to oxygen vacancy ordering, inside of which some nanometer sized domains show high-spin Co ions in the planes containing O vacancies and low-spin Co ions in the stoichiometric planes. First-principles calculations provide support for this interpretation.

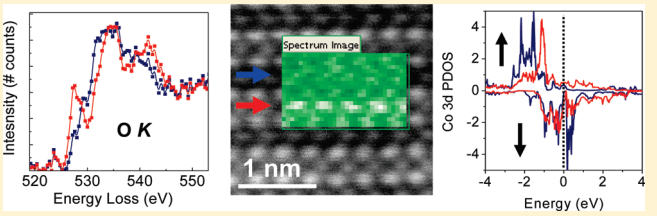

KEYWORDS: Cobaltites, spin state, O vacancies, electron energy loss spectroscopy

Cobalt oxides are relevant for a vast array of materials applications ranging from batteries to catalysts, thermoelectrics, electronics, spintronics, etc. Cobaltites with the perovskite structure are particularly interesting, since Co ions exhibit a competition between the crystal field splitting and Hund's rule exchange energy in the 3d states, which ultimately determines the spin state of the individual Co ions.[1−4] The ability to control spin states would offer new potential for tuning materials properties. However, spin states are sensitive to factors such as temperature, epitaxial strain, the precise environment of the Co atom, etc., and spin state configurations, and the ensuing transitions are far from understood.

Divalent ($3d^7$), trivalent ($3d^6$), or tetravalent ($3d^5$) Co ions in some bulk compounds such as nonperovskite cobaltites with unoccupied O sites exhibit various Co spin state superstructures.[1,3] These superstructures are generally observed using bulk magnetotransport, neutron scattering, X-ray diffraction, and other techniques that either provide reciprocal-space information or probe large real-space areas,[2,3,5] the nature of the spin state often being interpreted by means of density-functional theory (DFT) or quantum chemistry calculations.

However, these average techniques may not be sensitive to small domains or nanopockets, such as may occur within thin films under inhomogeneous degrees of epitaxial strain or with large amounts of defects not present in the bulk, e.g., interstitials or vacancies. Large concentrations of O vacancies are known to convert insulators to metals,[6] to induce ferromagnetism, and to form defect complexes with magnetic ions, producing room-temperature ferromagnetism in otherwise nonmagnetic oxides.[7] In Co oxides they can also affect the resulting Co spin state.[1−3,5,8−11] If such features are present as nanopockets they not only may affect the overall macroscopic system properties but also can point to new directions of synthesis to tune the properties of thin films and heterostructures.

In recent years, aberration correction in the scanning transmission electron microscope (STEM) has provided the capability of atomic-resolution Z-contrast imaging and electron-energy-loss spectroscopy (EELS), allowing simultaneous real space studies of structure, chemistry, and electronic properties.[12−15] It has even been shown that changes in the net spin of Co may have a fingerprint in the near edge fine structure of O K edges such as the case of $LaCoO_3$,[8] where the prepeak intensity changed when cooling through the 80 K spin-state transition, with the higher prepeak intensity found for the lowest spin state.[8] Meanwhile, the Co L_{23} ratio stayed constant, since the Co oxidation state does not change with temperature. Similar behaviors have been observed in average X-ray absorption spectra from bulk samples,[16] but EELS has the potential of real space atomic resolution mapping, which other techniques lack.

In this communication, we reveal a novel superlattice in the spin state of nanometer-sized regions with atomic resolution. Nanodomains of a cobaltite thin film can be highly oxygen deficient, probably reflecting nonuniformity in strain release. Important local structural changes may be present, to which average macroscopic techniques would not be sensitive. We use $La_{0.5}Sr_{0.5}CoO_{3-\delta}$ (LSCO), thin films, which, unlike the bulk, contain ordered arrays of O vacancies connected to the release of epitaxial strain.[17,18] Some nanometer size pockets in our films

Received: October 5, 2010
Revised: January 27, 2011
Published: February 10, 2011

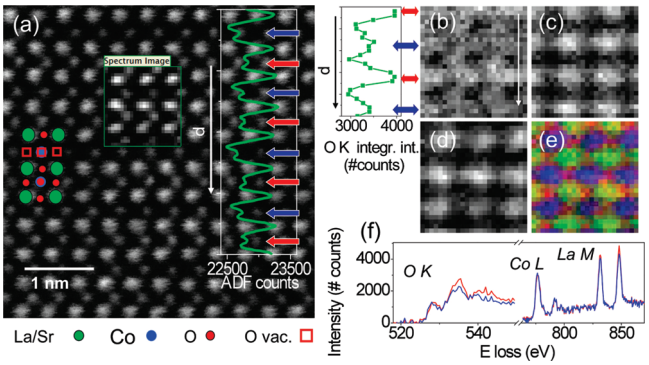

Figure 1. (a) *Z*-contrast image of a LSCO [001] film. The linetrace shows the ADF signal, averaged laterally. The bright/dark Co−O stripes are marked with red/blue arrows. The inset shows the region where a spectrum image 24 × 25 pixels wide was acquired, with an exposure time of 0.2 s per pixel, along with the simultaneous ADF signal. (b−d) Elemental maps corresponding to the O K, Co $L_{2,3}$, and La $M_{4,5}$ edges, respectively. Integration windows 30 eV wide were used after background subtraction using a power-law fit. For the La edge two fitting windows were used. The linetrace by (b) shows the averaged O K image intensity along the direction of the white arrow. (e) RGB map produced by overlaying the images in (b, red), (c, green), and (d, blue). (f) EEL spectra after background subtraction, averaged along the bright (red) and dark (blue) stripes. Data from the Nion UltraSTEM.

were found to have particularly low oxygen contents. While bulk LSCO does not exhibit Co spin state ordering, in these nanopockets we find a novel spin-state superstructure, with alternating high spin and low spin (HS/LS) Co ions in planes containing O vacancies vs fully oxygenated ones.

The films were deposited by reactive dc magnetron sputtering on $SrTiO_3$ (001) crystals (details can be found elsewhere[18]). After growth, the samples were cooled in a 500 Torr O_2 atmosphere but not subjected to the common postgrowth annealing step. Aberration-corrected STEM ADF imaging and EELS were acquired using a VG Microscopes HB501UX and a Nion UltraSTEM both operated at 100 kV and equipped with a Nion aberration corrector and an Enfina Gatan spectrometer. For spectrum imaging, the electron beam is scanned along the image region and in every pixel an EEL spectrum is acquired, along with the ADF signal. Specimens for STEM were prepared by conventional methods, by grinding, dimpling, and Ar ion milling. Calculations used density functional theory (DFT)[19] combined with the projector augmented wave (PAW) method[20] and spin-polarized generalized-gradient approximation (GGA) as implemented in the VASP code.[21,22]

The LSCO thin films are strained, tetragonally distorted, and show the typical domain structure induced during growth,[18] resulting from the ordering of O vacancies. Such ordering doubles the perovskite unit cell[23−26] and allows an elongation and distortion of the cell along the *c* axis to accommodate the mismatch with the substrate. Figure 1 displays a *Z*-contrast or annular dark-field (ADF) image with a magnified view of this superstructure. Every other Co−O plane shows a dimmer contrast as shown in the linetrace. This type of contrast is due to the ensuing structural relaxations, which promote the La/Sr planes to move further apart from the darker Co−O plane. This behavior has often been observed in perovskites, including cobaltites, ferrites, even cuprates such as YBCO, where the CuO chains show a significantly dimmer contrast than the CuO_2 planes. We will refer to these planes as dark Co−O planes or dark stripes.

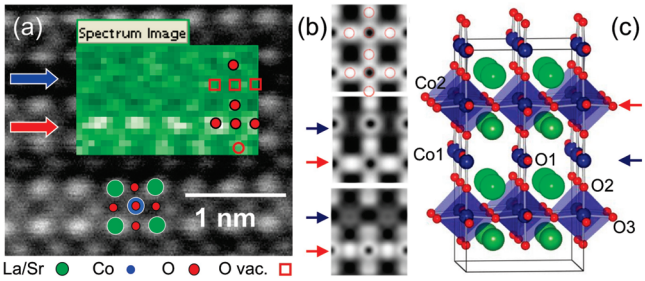

Figure 2. (a) Superstructure at higher magnification. Inset: area used for spectrum imaging along with the O K image (false color) generated by integrating PCA-treated spectra over a 30 eV window, after background subtraction. The acquisition time was 1.5 s per pixel. (b) O K edge simulated images down the [010] zone axis. The parameters used were defocused Δf = 62 Å, third and fifth order spherical aberration coefficients of −0.05 and 63 mm, a probe forming aperture of 23 mrad and a thickness, determined from low-loss spectra, of around 30 nm. (c) Sketch of the $La_{0.5}Sr_{0.5}CoO_{2.25}$ structure. Co2 is surrounded by a fully oxygenated octahedron, while each Co1 only has three nearest-neighbor oxygen vacancies. Blue (red) arrows point to the dark (bright) stripes. Data from the VG Microscopes HB501UX.

The small inset of Figure 1a shows the region where an EEL spectrum image was recorded along with the simultaneously acquired ADF signal. Panels b−d of Figure 1 show the atomic resolution maps of the O K, Co $L_{2,3}$, and La $M_{4,5}$ edges, around 530, 779, and 832 eV, respectively. Principal-component analysis (PCA) was used to remove the random noise from the EEL spectra.[27] Red and blue arrows mark the brighter and dimmer Co−O planes, respectively. The linetrace by Figure 1b shows the O K signal along the direction of the white arrow. The signal decreases on the dark Co−O stripes (see also the averaged spectra in Figure 1f, after background subtraction before the O K edge), consistent with the presence of O vacancies.

Final evidence of the presence of ordered O vacancies in these nanodomains comes from simulations. The experimental oxygen maps are only in good agreement with calculated dynamical images based on oxygen-depleted structural models.[28] Figure 2a shows another ADF image obtained from a nanodomain of the LSCO film with an unusually low local O content, along with the O K edge image acquired within the inset. Figure 2b shows the simulated EELS maps of the O K edge using the structures of three cobaltites: bulk oxygen stoichiometric perovskite $La_{0.5}Sr_{0.5}CoO_3$ (top), $La_{0.5}Sr_{0.5}CoO_{2.25}$ as reported by Wang et al.[26] (middle), and a structure (bottom), with the same oxygen stoichiometry as the previous one but different location of oxygen vacancies. This tetragonal structure, shown in Figure 2c, was implicated by the match between the experimental data and DFT calculations, shown below. The bottom simulation shows the best agreement with the experiment, better also than other simulations based, e.g., on the Brownmillerite structure. The fingerprint of O vacant sites is seen to be a dimmer peak located in the dark Co−O plane, where Co atoms are coordinated with just four O atoms. We will refer to Co on the dark stripe as Co1 and to Co on the bright Co−O plane as Co2. O1 is the O position in the dark Co−O plane and O3 is the O ion in the fully oxygenated Co−O plane.

This distribution of oxygen vacancies severely affects the local electronic properties of the Co atoms. The unoccupied density of states can be investigated by examining the fine structure of the Co $L_{2,3}$ and O K edges. Figure 3a shows the fine structure of these

dx.doi.org/10.1021/nl1034896 |*Nano Lett.* 2011, 11, 973–976

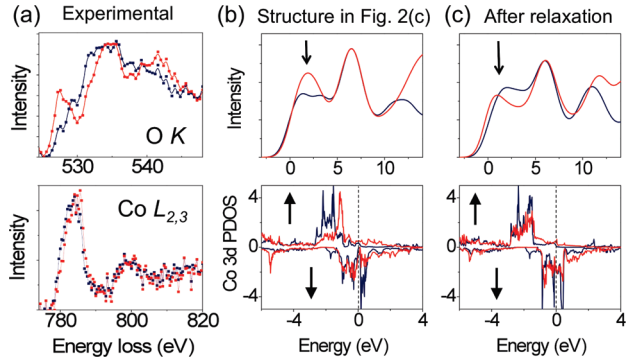

Figure 3. (a) Averaged O K and Co $L_{2,3}$ spectra from the bright stripe (red) and dark stripe (blue), scaled for presentation purposes. (b) Simulated O K edges for the O3 (red) and O1 (blue) atoms for the $La_{0.5}Sr_{0.5}CoO_{2.25}$ compound (top) along with the Co 3d PDOS for Co1 (blue) and Co2 (red) (bottom). (c) Calculations for the $La_{0.5}Sr_{0.5}CoO_{2.25}$ compound after relaxation. Vertical dashed lines mark the Fermi level position. Black arrows show the spin up and down channels in the PDOS.

edges averaged along the dark (blue) and bright (red) Co−O stripes of the data set in Figure 2, after normalization. The intensity ratio of the L_3 and L_2 lines of the Co $L_{2,3}$ edge (the $L_{2,3}$ ratio) correlates with the oxidation state of Co.[26] In this nanodomain the $L_{2,3}$ ratio measured was close to that of Co^{2+}. But more importantly, the Co $L_{2,3}$ ratio remains unchanged when shifting the electron beam from bright to dark Co−O stripes. Hence, there is *no change* in Co valence along the different Co−O planes (i.e., no charge ordering).

The O K edge fine structure, however, shows a significant decrease in the prepeak intensity along the dark stripe (blue spectrum in Figure. 3a). This pre-edge feature is sensitive to the filling of the hybridized O-2p and Co-3d states.[29] However the Co $L_{2,3}$ data rule out a different filling of the Co-3d band (i.e., Co oxidation state) between bright and dark stripes. To interpret these findings we turn to DFT. Simulations of the O K edges were performed using the $Z+1$ approximation.[30] Simulated O K edges of both the O1 and the O3 positions using the heavily deoxygenated $La_{0.5}Sr_{0.5}CoO_{2.25}$ structure in Figure 2c, with lattice constants of 0.375, 0.375, and 0.7275 nm, are shown in Figure 3b. While not identical, the simulated edges are consistent with the experimental data. A noticeably higher prepeak (arrow) on the O K edge is reproduced on the bright stripe. For this structure, the projected densities of states (PDOS) on both Co species are shown in the bottom panel. The total 3d band occupations for Co1 and Co2 are the same (the sum of the Co 3d orbital occupancies is 7.34 and 7.33 for Co1 and Co2 sites, respectively), consistent with the Co $L_{2,3}$ EELS data. But the PDOS on the Co1 and Co2 positions show noticeably different occupations of the spin up and spin down populations for the 3d bands (Table 1). While the Co2 configuration is consistent with a LS state, Co1 is in a HS state, with three down channels mostly empty. These configurations are consistent with the reduced Co measured from the L_{23} ratio (for pure Co^{2+} the HS and LS states have $S = 3/2$ and $S = 1/2$). Moments of 1.2 μ_B/Co for Co2 and 1.8 μ_B/Co for Co1 are predicted. These calculations demonstrate that an ordering of high densities of O vacancies along one of the Co−O planes can indeed stabilize a new spin-state-modulated structure. Since the changes in the simulated and experimental O K fine structures are similar, we conclude that the measured spatial modulation in the O K edge prepeak is the fingerprint for a spin-state superlattice in the nanodomain caused by the ordering of high concentrations of O vacancies.

Table 1. Co 3d Orbital Occupancies for Both Spin Up and Down Channels As Obtained from GGA Calculations[a]

		Co1		Co2	
		up	down	up	down
t_{2g}	xy	0.92	0.87	0.96	0.84
	yz	0.97	0.32	0.95	0.81
	zx	0.97	0.35	0.96	0.78
e_g	x^2-y^2	0.89	0.74	0.68	0.33
	$3z^2-r^2$	0.82	0.49	0.71	0.31

[a] Since Co1 is not in octahedral coordination the e_g/t_{2g} labels are only used as an "accounting" method.

The different possible spin states in cobaltites are determined by the competition of the Hund's rule exchange energy and the crystal field splitting.[2] For a fully octahedral symmetry the large crystal field, determined by the interaction with the nearest neighbor oxygen atoms, promotes a lower spin. If those nearest neighbors are absent and the symmetry is modified, a high spin state is favored, as observed in the Co1 species. Regarding the Co oxidation state, it should be noted that the films are metallic.[18] Although we cannot extract conclusions on the nanometric size pockets from averaged transport, the fact that the PDOS in Figure 3b does not show a gap indicates that these phases are probably still metallic. Hence charge ordering (i.e., valence ordering) is not expected.

Such a vacancy superstructure is only stabilized in the films by epitaxial strain. Theoretical support comes from allowing the structure in Figure 2c to fully relax. A different state is achieved, with around 0.15 eV lower energy. Lattice constants relax to 0.393, 0.371, and 0.789 nm, and the PDOS of Co1 and Co2 are no longer consistent with a spin-state ordering, both having a total magnetic moment of 2.1 μ_B per Co atom. Theoretical simulations of the O K edges for the relaxed structure in Figure 3c no longer show the large difference in prepeak structure from Figure 3a. Furthermore, the prepeak intensity is higher for the O1 atom (opposite to the experimental observation). Interestingly, this behavior is consistent with the O K data from the nanopocket of Figure 1f, denoting a partial, inhomogeneous strain release. These calculations confirm that the modulation of the O K edge fine structure observed in our data arises from a spin state superlattice and that the physics of these systems is extremely sensitive to local structural rearrangements and strain.

In summary, we report real-space atomic-resolution imaging of Co spin-state ordering in $La_{0.5}Sr_{0.5}CoO_{3-\delta}$ thin films. Unlike the bulk material, where no Co spin-state ordering is found, thin films present a strain-induced domain structure due to oxygen vacancy ordering, inside which some nanometer sized pockets show high-spin Co ions in the planes containing O vacancies, and low-spin Co ions in the stoichiometric planes. First-principles calculations provide support for this interpretation. The capability to image spin states with high spatial resolution may be relevant to the study of ferromagnetism in $LaCoO_3$ epitaxial films, since it is known to be highly sensitive to strain and structural changes too.[31−34] In fact, it is still unclear whether such magnetism is due to nonstoichiometry or if it is an intrinsic feature of the strained $LaCoO_3$ material itself. Our results pave the way to future real-space mapping of spin states around

dx.doi.org/10.1021/nl1034896 |*Nano Lett.* 2011, 11, 973–976

interfaces or defects in complex oxides and the tuning of properties through strain-stabilized spin state superlattices.

AUTHOR INFORMATION

Corresponding Author
*E-mail: jgazqueza@gmail.com.

ACKNOWLEDGMENT

The authors thank Julia Luck for STEM specimen preparation and Masashi Watanabe for the Digital Micrograph PCA plug-in. This work was supported by the Office of Science, Materials Sciences and Engineering Division of the US Department of Energy (W.L., S.J.P., M.V.), by DoE Grant FG02-09ER46554 (M.P.O., M.P.), and by the McMinn Endowment at Vanderbilt University (S.T.P.). J. Gazquez acknowledges financial support from the Spanish MEC 2007-0086 and European Research Council Starting Investigator Award, Grant #239739 STEMOX. Work at UMN was supported primarily by NSF (DMR-0804432) and DoE (DE-FG02-06ER46275, for neutron scattering characterization).

REFERENCES

(1) Khomskii, D. I.; Low, U. *Phys. Rev. B* **2004**, *69*, No. 184401.
(2) Khalyavin, D. D.; Argyriou, D. N.; Amman, U.; Yaremchenko, A. A.; Kharton, V. V. *Phys. Rev. B* **2007**, *75*, No. 134407.
(3) Doumerc, J. P.; Coutanceau, M.; Demourgues, A.; Elkaim, E.; Grenier, J.-C.; Pouchard, M. *J. Mater. Chem.* **2001**, *11*, 78–85.
(4) Imada, M.; Fujimori, A.; Tokura, Y. *Rev. Mod. Phys.* **1998**, *70*, 1039–1263.
(5) Maignan, A.; Caignaert, V.; Raveau, B.; Khomskii, D.; Sawatzky, G. A. *Phys. Rev. Lett.* **2004**, *93*, No. 026401.
(6) Herranz, G.; Basletic, M.; Bibes, M.; Carretero, C.; Tafra, E.; Jacquet, E.; Bouzehouane, K.; Deranlot, C.; Hamzic, A.; Broto, J.-M.; Barthelemy, A.; Fert, A. *Phys. Rev. Lett.* **2007**, *98*, No. 216803.
(7) Griffin-Roberts, K.; Varela, M.; Rashkeev, S.; Pantelides, S. T.; Pennycook, S. J.; Krishnan, K. M. *Phys. Rev. B* **2008**, *78*, No. 014409.
(8) Klie, R. F.; Zheng, J. C.; Zhu, Y.; Varela, M.; Wu, J.; Leighton, C. *Phys. Rev. Lett.* **2007**, *99*, 047203.
(9) Raccah, P. M.; Goodenough, J. B. *Phys. Rev.* **1967**, *155*, 932–943.
(10) Podlesnyak, A.; Streule, S.; Mesot, J.; Medarde, M.; Pomjakushina, E.; Conder, K.; Tanaka, A.; Haverkort, M. W.; Khomskii, D. I. *Phys. Rev. Lett.* **2006**, *97*, No. 247208.
(11) Phelan, D.; Louca, D.; Rosenkarnz, S.; Lee, S.-H.; Qui, Y.; Chupas, P. J.; Osborn, R.; Zheng, H.; Mitchell, J. F.; Copley, J. R. D.; Sarrao, J. L.; Moritomo, Y. *Phys. Rev. Lett.* **2006**, *96*, No. 027201.
(12) Browning., N. D.; Chisholm, M. F.; Pennycook, S. J. *Nature (London)* **1993**, *366*, 143–146.
(13) Varela, M.; Lupini, A.; Christen, H. M.; Dellby, N.; Krivanek, O. L.; Nellist, P. D.; Pennycook, S. J. *Phys. Rev. Lett.* **2004**, *92*, No. 095502.
(14) Bosman, M.; Keast, V. J.; Garcia-Muñoz, J. L.; D'Alfonso, A. J.; Findlay, S. D.; Allen, L. J. *Phys. Rev. Lett.* **2007**, *99*, No. 086102.
(15) Varela, M.; Luo, W.; Tao, J.; Oxley, M. P.; Watanabe, M.; Lupini, A. R.; Pantelides, S. T.; Pennycook, S. J. *Phys. Rev. B* **2009**, *79*, No. 085117.
(16) Abbate, M.; Fuggle, J. C.; Fujimori, A.; Tjeng, L. H.; Chen, C. T.; Potze, R.; Sawatzky, G. A.; Eisaki, H.; Uchida, S. *Phys. Rev. B* **1993**, *47*, 16124–16130. Haverkort, M. W.; Hu, Z.; Cezar, J. C.; Burnus, T.; Hartmann, H.; Reuther, M.; Zobel, C.; Lorenz, T.; Tanaka, A.; Brookes, N. B.; Hsieh, H. H.; Lin, H.-J.; Chen, C. T.; Tjeng, L. H. *Phys. Rev. Lett.* **2006**, *97*, No. 176405.
(17) Klenov, D. O.; Donner, W.; Foran, B.; Stemmer, S. *Appl. Phys. Lett.* **2003**, *82*, 3427–3429.
(18) Torija, M. A.; Sharma, M.; Fitzsimmons, M. R.; Varela, M.; Leighton, C. *J. Appl. Phys.* **2008**, *104*, No. 023901.
(19) Kohn, W.; Sham, L. J. *Phys. Rev.* **1965**, *140*, A1133–A1138.
(20) Blochl, P. E. *Phys. Rev. B* **1994**, *50*, 17953–17979.
(21) Kresse, G.; Furthmüller, J. *Phys. Rev. B* **1996**, *54*, 11169–11186.
(22) Perdew, J. P.; Burke, K.; Ernzerhof, M. *Phys. Rev. Lett.* **1996**, *77*, 3865–3868.
(23) Rao, C. N. R.; Gopalakrishnan, J.; Vidyasagar, K. *Indian J. Chem.* **1984**, *23A*, 265–284.
(24) Das, A.; Paranjpe, S. K.; Joy, P. A.; Date, S. K. *J. Alloys Compd.* **2001**, *326*, 101–104.
(25) Klie, R. F.; Ito, Y.; Stemmer, S.; Browning, N. D. *Ultramicroscopy* **2001**, *86*, 289–302.
(26) Wang, Z. L.; Yin, J. S. *Philos. Mag. B* **1998**, *77*, 49–65.
(27) Bosman, M.; Watanabe, M.; Alexander, D. T. L.; Keast, V. J. *Ultramicroscopy* **2006**, *106*, 1024–1032.
(28) Oxley, M. P.; Varela, M.; Pennycook, T. J.; Findlay, S. D.; D'Alfonso, A. J.; Allen, L. J.; Pennycook, S. J. *Phys. Rev. B* **2007**, *76*, No. 064303.
(29) Abbate, M.; de Groot, F. M. F.; Fuggle, J. C.; Fujimori, A.; Strebel, O.; Lopez, F.; Domke, M.; Kaindl, G.; Sawatzky, G. A.; Takano, M.; Takeda, Y.; Eisaki, H.; Uchida, S. *Phys. Rev. B* **1992**, *46*, 4511–4519.
(30) Buczko, R.; Duscher, G; Pennycook, S. J.; Pantelides, S. T. *Phys. Rev. Lett.* **2000**, *85*, No. 02168.
(31) Fuchs, D.; Arac, E.; Pinta, C.; Schuppler, S.; Schneider, R.; Löhneysen, H. v. *Phys. Rev. B* **2008**, *77*, No. 014434.
(32) Rondinelli, J. M.; Spaldin, N. A. *Phys. Rev. B* **2009**, *79*, No. 054409.
(33) Herklotz, A.; Rata, A. D.; Schultz, L.; Dörr, K. *Phys. Rev. B* **2009**, *79*, No. 092409.
(34) Mehta, V. V.; Liberati, M.; Wong, F. J.; Chopdekar, R. V.; Arenholz, E.; Suzuki, Y. *J. Appl. Phys.* **2009**, *105*, No. 07E503.